Electronic Supplementary Material (ESI) for Journal of Materials Chemistry C.


# Facile Template-free Preparation of Silver-coated $Cu_3SbS_4$ Hollow Spheres with Enhanced Photoelectric Properties

Xiang Meng[a], Xihao Chen[a, b], Jiang Cheng[a], Fuqiang Zhai[a], Wen Li[c], Rui Hu[d], Lu Li[a, *]

[a]*School of Material Science and Engineering, Chongqing University of Arts and Sciences, Chongqing 402160, China.*
[b]*Department of Physics, Chongqing University, Chongqing, 400044, China*
[c]*Interdisciplinary Materials Research Center, School of Materials Science and Engineering, Tongji Univ., 4800 Caoan Rd., Shanghai 201804, China*
[d]*Key Laboratory of Photovoltaic and Energy Conservation Materials, Institute of Solid State Physics, Hefei Institutes of Physical Science, Chinese Academy of Sciences, Hefei 230031, China*

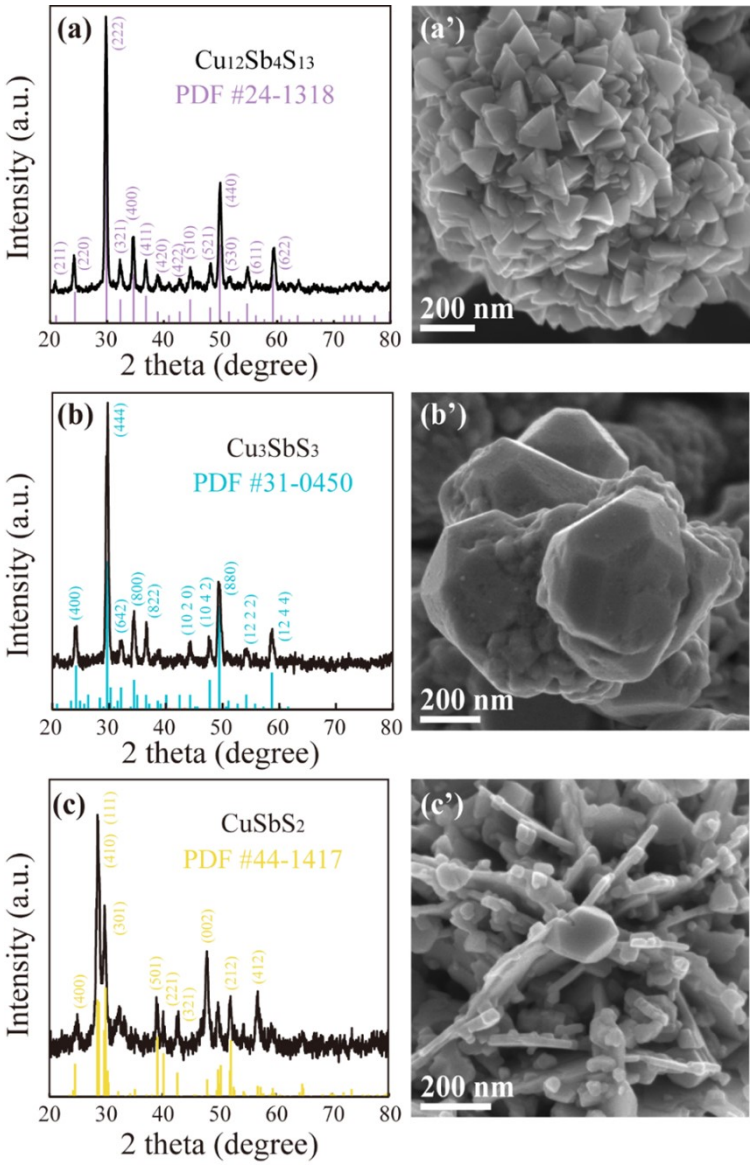


Figure S1. XRD patterns of the as-synthesized (a) $Cu_{12}Sb_4S_{13}$, (b)$Cu_3SbS_3$ and (c) $CuSbS_2$ by solvothermal method along with the standard reference pattern as #24-1318, #31-0450 and #44-1417, respectively, SEM images of (a') $Cu_{12}Sb_4S_{13}$, (b') $Cu_3SbS_3$ and (c') $CuSbS_2$. High-purity Cu-Sb-S phases were formed and distinguishing morphology (including configuration and size) could be recognized from SEM images.

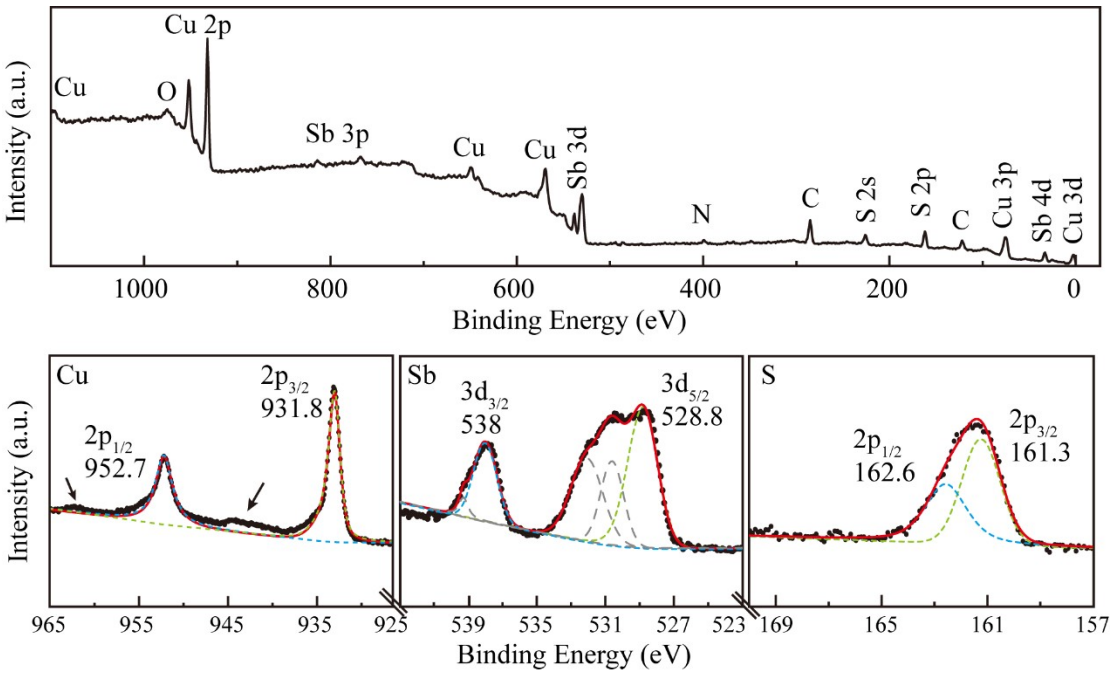


Figure S2. XPS spectra of the as-synthesized $Cu_{12}Sb_4S_{13}$ nanocrystals including the survey spectrum along with the corresponding high-resolution XPS spectra for Cu 2p, Sb 3d and S 2p core levels.

Calculation of Ag content:

The relative content of Ag and $Cu_3SbS_4$ in the composites can be calculated by the K value method, and the formula is described as follows[1]:

$I_A/I_S=k\times W_A/W_S$

Where I is the diffraction peak intensity, W is the weight percentage, and k is a constant value. The k value could be obtained from the standard PDF card. Both 0.5 vol% Ag and 1 vol% Ag content in the composites could be roughly estimated from XRD patterns.

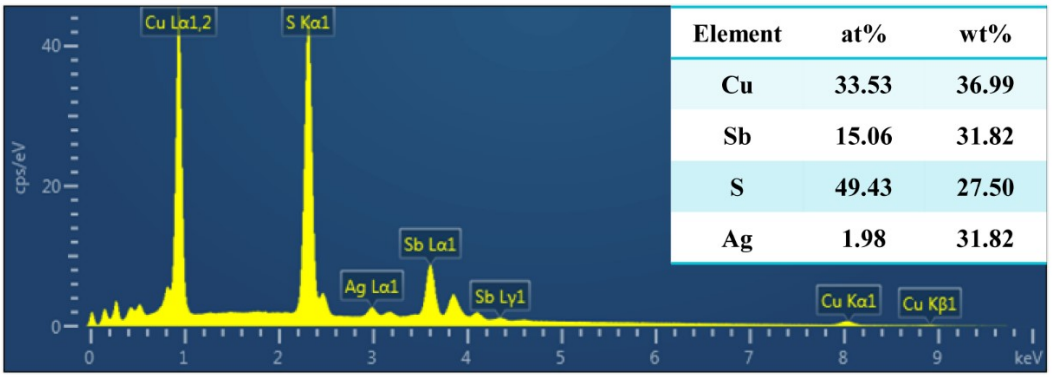


| Element | at% | wt% |
|---|---|---|
| Cu | 33.53 | 36.99 |
| Sb | 15.06 | 31.82 |
| S | 49.43 | 27.50 |
| Ag | 1.98 | 31.82 |

Figure S3. EDS result for the elemental mapping image along with the relative chemical composition of the as-synthesized Ag-coated $Cu_3SbS_4$ nanocrystals hollow spheres.

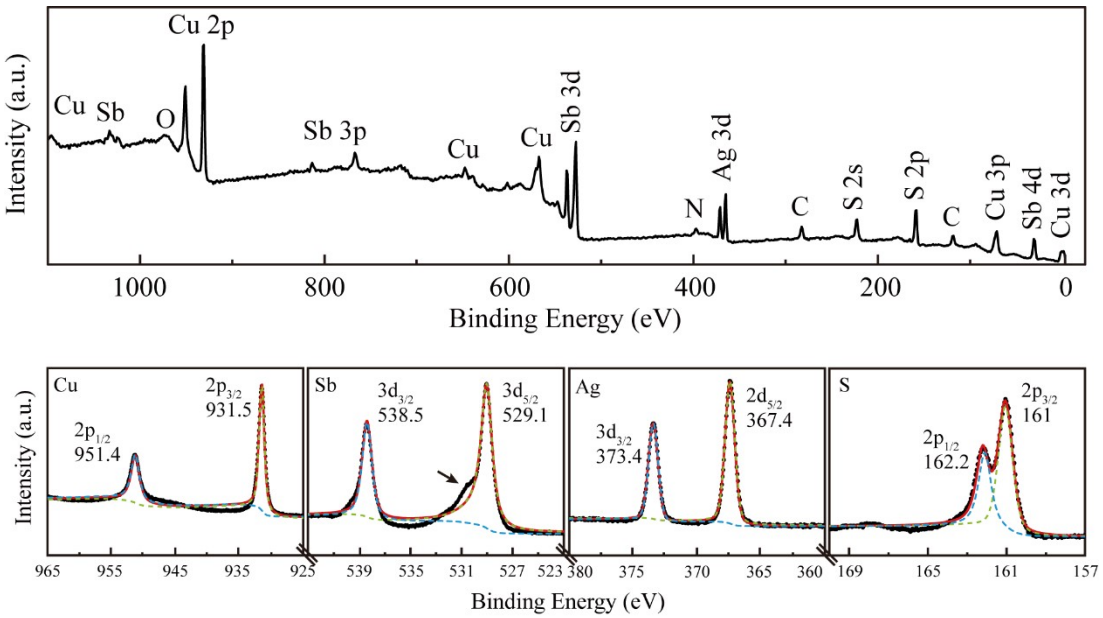


Figure S4. XPS spectra of the as-synthesized Ag-coated $Cu_3SbS_4$ nanocrystals hollow spheres including the survey spectrum along with the corresponding high-resolution XPS spectra for Cu 2p, Sb 3d, Ag 2d and S 2p core levels. A relatively small satellite peak at 530.6 eV appeared, which means a very little reduction of $Sb^{5+}$ into $Sb^{3+}$ by sodium borohydride. The change has not been mentioned in the main body due to a relatively small change.

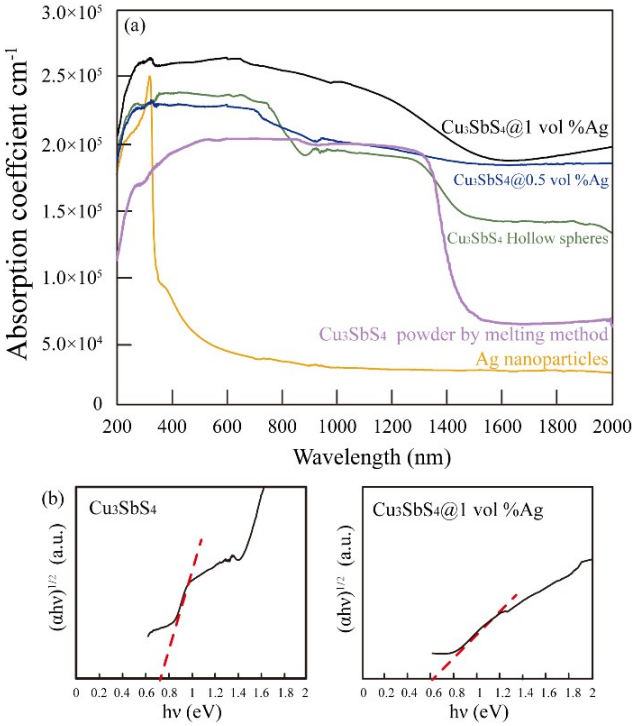


Figure S5. (a) UV-Vis-NIR spectra of Ag nanoparticles, $Cu_3SbS_4$ powder by melting method, $Cu_3SbS_4$ nanocrystals hollow spheres, 0.5 vol % Ag-coated $Cu_3SbS_4$ and 1 vol % Ag-coated $Cu_3SbS_4$, the corresponding Tauc plot of $(\alpha h\nu)^{1/2}$ versus ($h\nu$) of the as-synthesized (b) $Cu_3SbS_4$ nanocrystals hollow spheres and (c) Ag-coated ones.

Given the absorption spectrum of Ag clusters, the Ag nanoparticles with sphere structure possessed a broad peak at 400 nm for surface plasmon resonance[2]. The broad peaks located around 320 nm and 900 nm attributed to the in-plane dipole plasmon and out-of-plane quadrupole resonances, respectively, which suggested the formation of Ag with triangular nanoprism structure[3]. This could be possibly aroused from geometry of $Cu_3SbS_4$ nanoparticles precursor.

Calculation of optical band gap:
The optical bandgap of the film is determined from the absorption coefficient using

$$\alpha^m = A(h\nu - E_g) \quad (1)$$

where $A$ is a constant, $m$ is the transition probability, $E_g$ is the optical band gap[4]. The value of n could be 1/2 or 2 for allowed indirect or direct transitions, respectively. From the experimental results and theoretical calculations for band structure, $n = 1/2$ for $Cu_3SbS_4$ with an indirect transition was chosen[5–8].The bandgap of samples is determined from the plot of $(\alpha \cdot h\nu)^2$ versus photon energy by extrapolating to $\alpha \cdot h\nu = 0$.

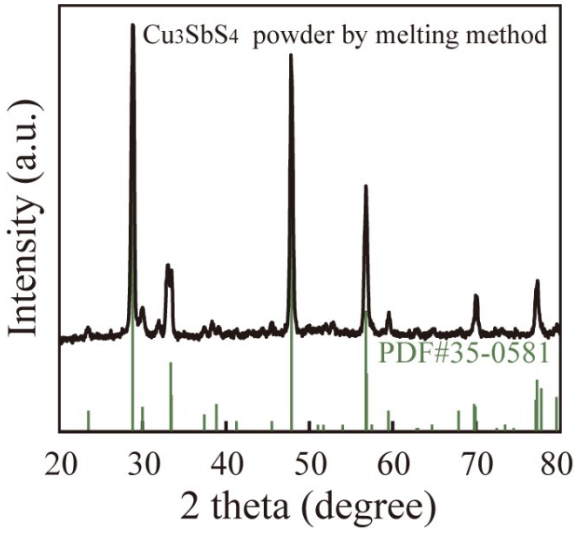


Figure S6. XRD pattern of the as-synthesized bulk $Cu_3SbS_4$ by melting method, a small quantity of $Cu_{12}Sb_4S_{13}$ was detected. Polycrystalline sample of $Cu_3SbS_4$ was synthesized by the stoichiometric amount of high purity elements (>99.99%) at 1173K for 24h, cooled down to 673K and held on for 2d. The obtained ingots were hand-ground into fine powder for hot pressing at 673 K for 20 min under a uniaxial pressure of 80 MPa.

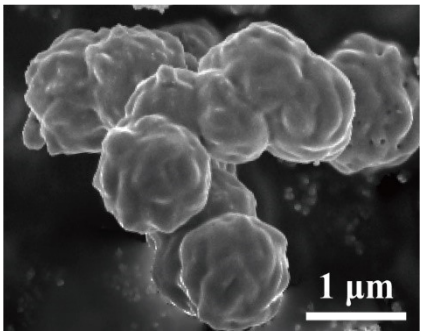


Figure S7. SEM images of the smaller spherical aggregation of crystals by only 5 min duration

time at high temperature

Table S1. The representative preparation method, structural properties and optical band gap (indirect) of $Cu_3SbS_4$

| Method | Size of crystals (nm) | Shape of crystals | Form | valence state | Optical band gap (eV) | Application | Ref. |
|---|---|---|---|---|---|---|---|
| Solvothermal method | 200 | - | Powder | | 1 | - | 9 |
| Solvothermal method | 26-32 | sphere | Powder | | 0.88-1 | - | 10 |
| Solvothermal method | 20 | - | Film (SC) | | 0.82 | - | 11 |
| hydrothermal | 40-60 in thickness | nanofibers | Powder | | - | - | 12 |
| Hot-injection | 10.2±1.1 | spherical | Powder | 1 3 2 | 0.9 | - | 6 |
| Hot-injection | 10 | spherical | Powder | 1 3 2 | 1 | - | 13 |
| Hot-injection | 10.5±1.7 | spherical | Powder | | 1.72 | - | 14 |
| Hot-injection | 23±4 | oblates | Powder | | 1.2 | - | 5 |
| Hot-injection | 61±19 | irregular to tetragonal | Powder | 1 3 2 | 1.33 | - | 15 |
| Hot-injection | 5.95±0.67 | dots | Powder | | 1.5 | - | 7 |
| | 4.81±0.52 | | | | 1.6 | | |
| | 3.37±0.46 | | | | 1.7 | | |
| Hot-injection | 4.72±0.52 | Quasi-spherical | Powder | | 1.4 | For optoelectronic devices | 16 |
| Hot-injection | 14-20 | - | Film (spray deposited method using chlorobenzene) | | 0.89 | Hole transporting material in solar cells | 17 |
| Hot-injection | 21.5±8.0 | Round-like | Powder | | ≥1 | - | 8 |
| Hot-injection | 19 | - | Film (SC) | 1 5 2 | 0.9 | Absorber layer in TFSC | 18 |
| Microwave radiation | 30-50 | sphere-like | Powder | 1 5 2 | 1.1 | - | 19 |
| Mechanical alloying with spark plasma sintering | ≥1000 | - | Powder | 1 5 2 | 0.85 | Thermoelectric materials | 20 |
| Deep eutectic solvents synthetic approach | ~7 | nearly spherical | - | 1 5 2 | 1.23 | Water-splitting | 21 |
| RF magnetron sputtering with Sulfurization | ≥1000 | - | Film | | 0.89±0.01 | - | 22 |
| Electron-beam evaporation with Sulfurization | ≥1000 | - | Film | | 0.88 | - | 23 |
| Magnetron | 50±30 | - | Film | | 0.94-0.97 | For TFSC | 24 |

| | |
|---|---|
| | sputter with Sulfurization |

Where, TFSC is the abbreviation for thin film solar cells, SC is the abbreviation for spin-coating, ≥1000 means that the size of crystals was calculated roughly by us from SEM results in these papers and close to micrometer. The form is the state of $Cu_3SbS_4$ when the UV-Vis measurement was conducted. Three numbers in valence state column are corresponding to valence states of element Cu, Sb and S in $Cu_3SbS_4$, respectively.

Reference:


1 C. R. Hubbard and R. L. Snyder, *Powder Diffr.*, 1988, **3**, 74–77.
2 H. Bi, W. Cai, L. Zhang, D. Martin and F. Träger, *Appl. Phys. Lett.*, 2002, **81**, 5222–5224.
3 J. Liu, X. Li and X. Zeng, *J. Alloys Compd.*, 2010, **494**, 84–87.
4 E. A. Davis and N. F. Mott, *Philos. Mag.*, 1970, **22**, 0903–0922.
5 K. Ramasamy, H. Sims, W. H. Butler and A. Gupta, *Chem. Mater.*, 2014, **26**, 2891–2899.
6 J. van Embden and Y. Tachibana, *J. Mater. Chem.*, 2012, **22**, 11466.
7 K. Chen, J. Zhou, W. Chen, Q. Chen, P. Zhou and Y. Liu, *Nanoscale*, 2016, **8**, 5146–5152.
8 F. Baum, T. Pretto, A. G. Brolo and M. J. L. Santos, *Cryst. Growth Des.*, 2018, **18**, 6521–6527.
9 L. Shi, C. Wu, J. Li and J. Ding, *J. Alloys Compd.*, 2017, **694**, 132–135.
10 J. Bincy, G. S. G. and L. R. A., *Mater. Res. Bull.*, 2017, **95**, 267–276.
11 M. Bella, C. Rivero, S. Blayac, H. Basti, M. C. Record and P. Boulet, *Mater. Res. Bull.*, 2017, **90**, 188–194.
12 C. An, Y. Jin, K. Tang and Y. Qian, *J. Mater. Chem.*, 2003, **13**, 301–303.
13 J. van Embden, K. Latham, N. W. Duffy and Y. Tachibana, *J. Am. Chem. Soc.*, 2013, **135**, 11562–11571.
14 S. Ikeda, S. Sogawa, Y. Tokai, W. Septina, T. Harada and M. Matsumura, *RSC Adv*, 2014, **4**, 40969–40972.
15 Q. Liang, K. Huang, X. Ren, W. Zhang, R. Xie and S. Feng, *CrystEngComm*, 2016, **18**, 3703–3710.
16 F. Zhang, K. Chen, X. Jiang, Y. Wang, Y. Ge, L. Wu, S. Xu, Q. Bao and H. Zhang, *J. Mater. Chem. C*, 2018, **6**, 8977–8983.
17 Q. Zeng, Y. Di, C. Huang, K. Sun, Y. Zhao, H. Xie, D. Niu, L. Jiang, X. Hao, Y. Lai and F. Liu, *J. Mater. Chem. C*, 2018, **6**, 7989–7993.
18 G. H. Albuquerque, K.-J. Kim, J. I. Lopez, A. Devaraj, S. Manandhar, Y.-S. Liu, J. Guo, C.-H. Chang and G. S. Herman, *J. Mater. Chem. A*, 2018, **6**, 8682–8692.
19 G. Chen, W. Wang, J. Zhao, W. Yang, S. Chen, Z. Huang, R. Jian and H. Ruan, *J. Alloys Compd.*, 2016, **679**, 218–224.
20 M. Shen, S. Lu, Z. Zhang, H. Liu, W. Shen, C. Fang, Q. Wang, L. Chen, Y. Zhang and X. Jia, *ACS Appl. Mater. Interfaces*, 2020, **12**, 8271–8279.
21 U. V. Ghorpade, M. P. Suryawanshi, S. W. Shin, X. Wang, E. Jo, H. Bae, K. Park, J.-S. Ha, S. S. Kolekar and J. H. Kim, *J. Mater. Chem. A*, 2018, **6**, 19798–19809.
22 P. A. Fernandes, A. Shongalova, A. F. da Cunha, J. P. Teixeira, J. P. Leitão, J. M. V. Cunha, S. Bose, P. M. P. Salomé and M. R. Correia, *J. Alloys Compd.*, 2019, **797**, 1359–1366.
23 L. Yu, R. S. Kokenyesi, D. A. Keszler and A. Zunger, *Adv. Energy Mater.*, 2013, **3**, 43–48.
24 N. D. Franzer, N. R. Paudel, C. Xiao and Y. Yan, in *2014 IEEE 40th Photovoltaic Specialist Conference (PVSC)*, IEEE, Denver, CO, USA, 2014, pp. 2326–2328.